Axial Flux PMSM Power Take-Off for a Rim-Driven Contra-Rotating Pump-Turbine

Daan P. K. Truijen, Jeroen D. M. De Kooning, Dieter Fauconnier, Hendrik Vansompel, Peter Sergeant and Kurt Stockman
Department of Electromechanical, Systems & Metal Engineering, Ghent University, Ghent, Belgium
and *FlandersMake@UGent - Corelab EEDT-MP*, Belgium
Corresponding author: daan.truijen@ugent.be

***Abstract*—Pumped hydropower storage (PHS) is a cost-effective and mature energy storage technology. However, it has inherently been limited to locations with suitable topographies. Therefore, the ALPHEUS project aims to implement PHS for shallow seas and coastal environments with the goal to support grid stability. To ensure optimal efficiency and fast switching times in these low-head applications, a 10 MW Contra-Rotating (CR) axial Reversible Pump-Turbine (RPT) is designed, which has a rim diameter of 6.4 m and a high efficiency - maximum 84% and 90% for pump and turbine, over a large operating range. Furthermore, the RPT is rim-driven, which averts the hydraulic impact caused by shaft-driven systems. To ensure optimal efficiency at variable speed operation, the runners are driven by two separate Axial-Flux Permanent Magnet Synchronous Machines (AF-PMSMs). This paper proposes a Power Take-Off (PTO) design, where the electric machines and bearings are integrated in the rim of the CR RPT. The AF-PMSM dimensional design results in an outside diameter of 6.87 m. Next, active hydrostatic bearings are proposed due to their higher lifetime compared to roller bearings and better start-stop behaviour compared to hydrodynamic bearings. Finally, the advantages of the rim-driven PTO design with AF-PMSMs are elucidated by means of a comparison with the PTO of a shaft-driven CR RPT with similar power ratings. Next to the differences in hydraulic impact and bearing and sealing complexity, the active mass of both PTOs is examined. It is shown that the rotary mass and the total mass the rim-driven PTO is respectively three times and six times lower than that of the shaft-driven PTO, while the permanent magnet usage for both PTOs remains similar, with the total permanent magnet mass being 1.1% lower for the rim-driven PTO.**

***Index Terms*—Drivetrain, Axial-Flux PMSM, Hydropower, Power take-off**

I. Introduction

Pumped Hydropower Storage (PHS) is an established and cost-efficient technology. In the ALPHEUS project, Reversible Pump-Turbines (RPT) and adjacent technologies are improved to make low head PHS economically viable [1]. A 10 MW system is designed that is highly efficient and has low mode switching times, to allow to provide grid ancillary services. One of the investigated RPTs is a rim-driven Contra-Rotating (CR) RPT. Here, the two runners have opposite rotational motion, which limits the creation of swirl behind the RPT, thus increasing efficiency [2], improving pump stability and suppressing cavitation [3]. The two runners are driven at their rim by two separate electric machines. Therefore, the use of conventional shafts is averted, alleviating the impact of the Power Take-Off (PTO) on the hydraulic flow and increasing the total hydraulic efficiency.

Axial Flux Permanent Magnet Synchronous Machines (AF-PMSMs) can achieve a strong flux linkage due to a very small air gap and are suitable for low-speed-high-torque operations [4], [5]. A high pole number averts reduction gearing and the accompanying friction losses [6]. Due to their high torque density, efficiency and high diameter-to-length ratio [4], the implementation of AF-PMSMs for rim-driven turbines or pumps has recently been investigated in projects on marine current turbines [7] and ship propulsion systems [8]. Djebarri et al. implemented a Double-Stator AF-PMSM on a marine current turbine with a diameter of 11 m and rated power of 300 kW [9], [10]. Next to a detailed linear electromagnetic and thermal analysis, they compared the resulting AF-PMSM design to a radial-flux PMSM for the same application. Their findings showed a reduction in machine diameter and axial length of respectively 2% and 13% [10]. In this research, a double rotor AF-PMSM with Yokeless and Segmented Armature (YASA) topology is used. This topology compensates undesired axial forces and has no stator yoke, thus reducing iron losses and weight [11]. In this paper, the 10 MW rim-driven CR RPT is first analysed in section II. In section III, the rim-driven PTO is described. The PTO includes the positioning and dimensioning of electric machines, bearings and seals and is designed to manage the runner weight and torque, as well as the axial forces, while preserving optimal system performance. Finally, in section IV, the advantages of the derived rim-driven PTO design are elucidated by means of a comparison with a shaft-driven PTO of similar power ratings and dimensions.

II. Rim-Driven Contra-Rotating Reversible Pump-Turbine

Rim-driven propellers are found in a number of fields including hydropower, pumped hydropower storage, marine current applications and propulsion systems. The main benefit of rim-driven propellers compared to shaft-driven propellers is the absence of a shaft and PTO in the hydraulic flow. Therefore, the accessory hydraulic losses are averted, and the total hydraulic efficiency is increased. In order to use PHS to provide ancillary services for the grid in regions

This research is part of the ALPHEUS project and is funded by the European Union's Horizon 2020 research and innovation programme, grant agreement No 883553.

978-1-6654-6738-4/22/$31.00 ©2022 IEEE

with a flat topography, a rim-driven CR RPT is developed, which has increased efficiency at low head [2]. Furthermore, it can improve pumping stability at low flow rate and suppress cavitation at high flow rate [3]. In the ALPHEUS project, an initial design of the CR rim-driven RPT is developed by Advanced Design Technology Ldt., using ADT's TURBOdesign suite [12], based on a 3D inverse design method [13]. Table I lists the relevant properties for the 10 MW rim-driven design. The RPT geometries are shown in Fig. 1, with the main parameters indicated. Note that the axial gap between the rotors is magnified for better visualisation and is 0.25 m in reality. Evaluation with computational fluid dynamics results in a high efficiency - maximum 84% and 90% for pump and turbine mode respectively - over a large range of heads and flow rates. Finite element analysis confirms that the maximum von-Mises stress occurs at the shroud of the runners, with a maximum value of 154 MPa, which is far below the yield strength 1020 MPa of the used material Stainless Steel 17-4 H1075.

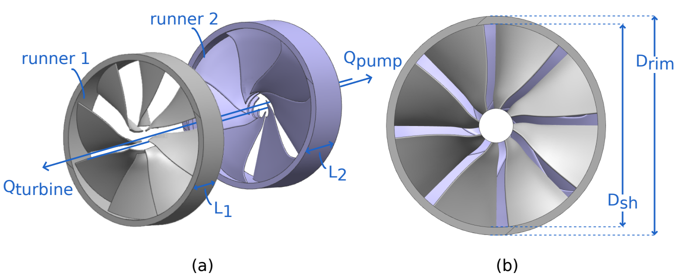

Fig. 1. Developed rim-driven contra-rotating RPT, with main parameters indicated on (a) trimetric view with magnified axial gap and (b) front view.

TABLE I
MAIN CR RPT PROPERTIES

	Symbol	Runner 1	Runner 2
Nominal rot. speed	Ω_{nom} [rpm]	50	-50
Rim diameter	D_{rim} [m]	6.40	6.40
Shroud diameter	D_{sh} [m]	5.94	5.94
Axial length	L [m]	1.30	1.70
Runner mass	m [kg]	$5.94 \cdot 10^4$	$7.75 \cdot 10^4$
Rotational inertia	J [kg m²]	$4.89 \cdot 10^6$	$6.39 \cdot 10^6$
Maximal axial force	$F_{a,\text{max}}$ [kN]	$1 \cdot 10^3$	$1.5 \cdot 10^3$

III. POWER TAKE-OFF CONCEPT

In this section, the Power Take-Off (PTO) design is analysed. First, the general concept is described in section III-A. Next, the AF-PMSM design is discussed in section III-B, followed by the analysis of bearings and sealing in section III-C.

A. General Concept

In this rim-driven PTO, Axial-Flux PMSMs (AF-PMSMs) are used due to their high efficiency and high diameter-to-length ratio. With the YASA topology, undesired axial forces on the rotor discs are averted and the flux path becomes predominantly axial due the North-South arrangement between the rotors. The axial flux path obviates the magnetic purpose of the stator yoke, further reducing iron losses and weight. It also allows for the use of grain-oriented steel in the stator teeth. This anisotropic material has a high permeability and low magnetic losses in the axial direction, increasing the efficiency [14]. Other efficiency improvements are achieved by using segmented permanent magnets and concentrated stator windings [11]. As pictured in Fig. 2, to reduce magnetic losses, both stator teeth and rotor magnets are formed by multiple rectangular segments that approximate an isosceles trapezium.

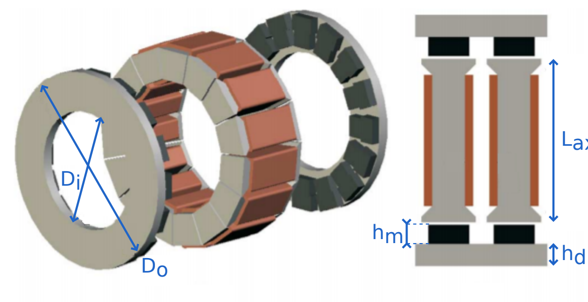

Fig. 2. YASA topology AF-PMSM with dimensional parameters indicated on (a) trimetric view with magnified axial air gap and (b) section view of the stator teeth at a constant radius [11].

Fig. 3 shows the proposed PTO design. The electric machines are directly coupled to the RPT runners via the rotor discs. Therefore, no gearbox is present, which averts the accompanying friction and increases reliability [6]. Using two separate electric machines allows for a variable speed ratio between the runners to allow efficient and dynamic response to grid state changes. Note that the inner tube diameter is equal to the RPT shroud diameter D_{shroud}. The runners are each supported by two sets of both a radial and an axial active hydrostatic bearing to carry both radial and axial forces.

B. AF-PMSM Design

Equation (1) shows the AF-PMSM power equation [15]. In this PTO design, two AF-PMSMs of 5 MW are used. Note that, in contrast to other common machines, the axial length of the AF-PMSM stator does not directly influence the electromagnetic torque. Therefore, the axial length of AF-PMSMs is relatively short and in this design $L_{\text{ax}} = 0.4$ m.

$$P = \frac{\pi^2\ \Omega_{\text{nom}}\ k_D\ k_w\ B_{mg}\ A_m\ D_o^3}{60} \tag{1}$$

In this equation k_D is the diameter ratio factor, k_w is the winding factor, $B_{mg} = 0.8\ T$ is the peak value of magnetic flux density in the air gap, D_o is the rotor magnets outer diameter and A_m is the linear current density in the air gap. The diameter ratio factor and winding factor, which combines distribution and pitch factor, are calculated as follows [15]:

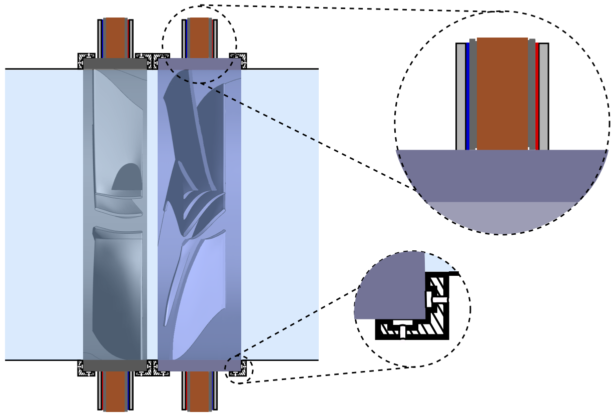

Fig. 3. General PTO concept, with the YASA topology AF-PMSM and active hydrostatic bearings positioned around the RPT periphery.

$$k_D = \frac{1}{8}\left(1+\frac{D_i}{D_o}\right)\left(1-\left(\frac{D_i}{D_o}\right)^2\right) \quad (2)$$

$$k_w = \frac{\sin(\frac{\pi}{2\cdot m_1})}{n\ q\ \sin(\frac{\pi}{2\cdot m_1\ n\ q})}\cdot \sin\left(\frac{p\ \pi}{Q_s}\right) \quad (3)$$

In (2), D_i is the inner diameter of the rotor magnets. In the proposed rim-driven PTO, $D_i = D_{\mathrm{rim}} = 6.4$ m. In (3), it is shown how the winding factor depends on the number of phases $m_1 = 3$, the number of stator slots Q_s, the number of poles p and number of stator-slots-per-pole-per-phase q. n is the denominator of q reduced to lowest terms. To reduce the torque ripple in permanent magnet machines with fractional slot windings, the relation between the number of stator slots and number of rotor poles has been an interesting topic for recent research. It is found that combinations with the same stator slots-per-phase-per-pole number q share the same winding factors k_w and harmonics in the torque characteristics [16], [17]. It was concluded that $1/4 < q < 1/3$ yields optimal torque characteristics while maintaining high winding factors [16]. Therefore, $q = 2/7$ is chosen in this design, which has a more sinusoidal electromagnetic torque compared to commonly used $q = 2/5$ and $q = 3/8$ arrangements, while maintaining low leakage inductance [18]. Due to the low nominal speed of the runners, the AF-PMSM rotors consist of 63 polepairs, making the nominal frequency $f_{\mathrm{nom}} = 52.5$ Hz. This ensures that the frequency is well below the power converter switching frequency. For commercially available converters in the megawatt range using IGBTs, the switching frequency typically is 500 Hz [19], although it was shown that a better trade-off between torque response, switching losses and power density is found at 1.5 kHz for power plants up to 10 MW [20]. With $p = 63$, the number of stator slots, using $q = 2/7$, becomes $Q_s = q \cdot m_1 \cdot 2p = 108$. With these parameters, k_w (3) can be caluclated $k_w = 0.933$. Now, D_o can be found as a function of the rated power $P = 5$ MW and A_m. A_m can range from 30 - 80 kA/m for air cooling to 150 - 200 kA/m for direct water cooling [21]. For a machine with effective air cooling, D_o can be reduced to 6.87 m. By using water cooling, the diameter can be further decreased to $D_o < 6.66$ m. However, due to the complexity of a cooling circuit that effectively reduces heat in the stator windings and air gap, this option is omitted in this high diameter AF-PMSM. Other parameters that are important for sizing purposes of the PTO are the air gap thickness $g = 5$ mm, the magnet thickness $h_m = 5$ mm and the rotor discs thickness h_d. The minimal rotor disc thickness to prevent rotor saturation, can be calculated as follows [9]:

$$h_{\mathrm{d,min}} = \frac{b_m}{2}\frac{B_{\mathrm{mg}}}{B_{\mathrm{d,max}}} \quad (4)$$

$$b_m = \beta_m \frac{\pi(D_i + D_o)/2}{p}$$

Here, b_m is the magnet width, β_m is the magnet pole pitch ratio and $B_{\mathrm{d,max}}$ is the maximal flux density of the rotor material, which is upwards of 1.5 T for standard construction steels, e.g. S235. Therefore, $h_d = 84$ mm. The total length of the proposed AF-PMSM becomes $L_{\mathrm{AF}} = L_{\mathrm{ax}} + 2 \cdot (g + h_m + h_d) = 0.59$ m, thus occupying only part of the axial length L of the RPT runners, which are listed in Table I.

The rotor mass m_r and rotational inertia of the PTO J_r, comprising the AF-PMSM rotors and magnets are given by respectively (5) and (6), where $\rho_{\mathrm{NdFeB}} = 7500$ kg/m³ and $\rho_{\mathrm{S235}} = 7800$ kg/m³ are the mass densities of the permanent magnets and the rotor S235 steel discs respectively. It is found that $m_r = 6.8 \cdot 10^3$ kg and $J_r = 7.5 \cdot 10^4$ kg m².

$$m_r = 2 \cdot (m_m + m_d) \quad (5)$$

$$m_m = \beta_m \rho_{\mathrm{NdFeB}} h_m \pi \left(\frac{D_o^2}{4} - \frac{D_i^2}{4}\right)$$

$$m_d = \rho_{\mathrm{S235}} h_d \pi \left(\frac{D_o^2}{4} - \frac{D_i^2}{4}\right)$$

$$J_r = 2 \cdot \frac{m_m + m_d}{2}\left(\frac{D_o^2}{4} + \frac{D_i^2}{4}\right) \quad (6)$$

C. Bearings and Sealing Selection

Bearings constrain the position of the RPT both radially and axially, while inducing minimal friction within the operating range (see Table I). Therefore, it must compensate for both the radial and axial forces of the RPT. As can be seen in Fig. 3, in absence of a shaft in a rim-driven RPT, the bearings are positioned around the periphery of the RPT and have a diameter of 6.4 m. Therefore, developing a bearing arrangement for this rim-driven PTO is a challenging objective.

To select the bearing type and arrangement, two main categories are distincted i.e., roller bearings and plain fluid bearings. These bearing types respectively use rolling elements and pressurised lubricant to carry loads, while allowing relative motion. In most turbines today, roller bearings are used as main bearings due to their high efficiency, suitability for low-speed applications and the absence of a high starting torque, which allows for frequent start-stops. Furthermore, the standardisation of main roller bearings has experienced a significant increase since the late 2000's. However, in wind applications, it has been found that these bearings do not meet the lifetime of the turbine. According to a study of over 2000 wind turbines of 1.5 to 2.5 MW, the main bearings have a failure rate of up to 30% over a 20 year period [22]. In addition, main bearing faults propagate to the electric machine in direct drive turbines, as no gearbox is present. Therefore, main bearing failures not only induce costs due to downtime and replacement of the bearing itself, but causes extra costs for maintenance and eventual replacement of electric machines. Furthermore, a roller bearing with an inner diameter of 6.4 m might be economically unsuitable, due to the significantly increased number of rolling elements and material, manufacturing and engineering costs.

Plain fluid bearings are a valuable alternative to roller bearings. In hydrodynamic bearings, a hydrodynamic pressure build-up is established in the lubricant film in the converging gap between the bearing shell and the eccentric shaft, due to the rotational motion of this shaft. Hydrodynamic bearings generally have a higher lifetime, lower cost and exhibit a damping effect that compensates for sudden force deviations. The main drawbacks of hydrodynamic bearings are lower efficiency compared to roller bearings and high starting torque, due to the rotation dependent lubricant film thickness. Traditionally, a hydrodynamic bearing arrangement that compensates both radial and axial forces consists of two separate bearings; one radial bearing and one axial thrust bearing. Large axial thrust bearings typically consist of tilting pads, attached to the bearing housing. A hydrodynamic pressure is established in the lubricant film, that is formed in the converging wedges between the tilting pads and the shaft. Therefore, the same effect is achieved as in a radial bearing. Recently, innovative combined (radial and axial) hydrodynamic bearings are developed for wind turbine applications. Here, common geometries of combined roller bearings, such as the double tapered roller bearing or toroidal bearing form the basis of the design [23].

As described above, in both radial and axial thrust hydrodynamic bearings, the lubricant film is established due to a sufficiently high rotational motion for a given lubricant viscosity, so that external forces can be accommodated. However, when the rotational speed of the shaft decreases, the lubricant film thickness decreases, narrowing the gap between the shaft and the bearing shell. For very low rotational speeds, e.g. during start-stop events, the film thickness is insufficient to fully separate the opposing surfaces, causing direct contact between the shaft and the shell. Besides a significant increase of friction, increasing start-up torque, such start-stop events induce wear and when occurring frequently, decrease the bearing lifetime. Especially when providing ancillary services to the grid, frequent start-stops are prominent. For these types of applications, recent research proposes active hydrostatic bearings, otherwise called hybrid bearings [24], [25]. In a hydrostatic bearing, the lubricant pressure is not provided by the shaft rotational speed, but by external pumps. The bearing comprises different chambers in which the pressurised lubricant is pumped. However, passive hydrostatic bearings are not suited for high shaft surface velocities, due to heating of the lubricant. Therefore, active hydrostatic bearings monitor this velocity and control the lubricant pressure accordingly. They combine the benefits of hydrodynamic bearings at nominal rotational speed and the benefits of hydrostatic bearings at standstill and start-stops. However, these bearings need an auxiliary high pressure pump unit and control architecture, that both increases initial price and requires energy consumption. Nonetheless, for a high diameter rim-driven CR RPT providing ancillary services, the application of active hydrostatic bearings is favorable. Their integration in the rim-driven PTO is pictured in Fig. 3. Each runner is supported by two radial and two axial bearings, optimally countering both the unidirectional radial load and the reversible axial loads.

To guarantee minimal water leakage between the RPT and the PTO housing, large diameter shaft seals must be installed around the RPT periphery. In hydropower installations, axial mechanical face seals are typically used. Here, a static carbon ring is spring loaded to a flange-type extension of the rotating shaft, commonly stainless steel, bronze or ceramic [26]. However, carbon sizes are limited, resulting in a segmented face ring, which complicates alignment between the sealing faces, increasing wear and leakage. Therefore, elastic polymer face rings are recently developed to replace the carbon, which can be machined for high diameters and increase resistance to abrasive wear [26]. Still, the complexity and cost of these large mechanical face seals is evident, as achieving face ring tolerances and spring loading across the periphery becomes more difficult for increasing diameters.

IV. Comparison with the PTO of Shaft-Driven Contra-Rotating RPT

In this section, the derived PTO is evaluated based on a comparison with the PTO design of a shaft-driven CR RPT with similar design and load conditions, which was proposed in [27]. A 3D CAD drawing of the PTO with optimised shaft dimensions is shown in Fig. 4. The PTO consists of two coaxial shafts, which allows the AF-PMSM to be placed on one side of the RPT, housed in a bulb.

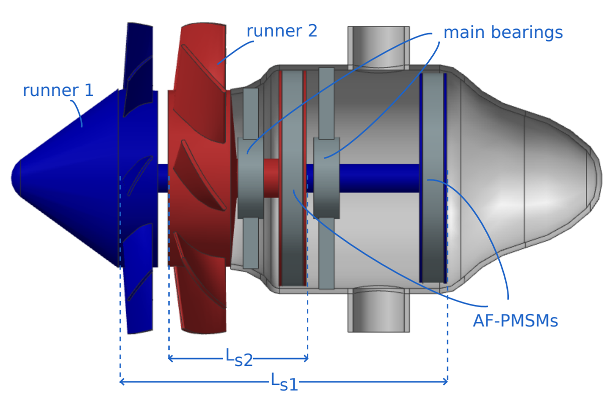

Fig. 4. 3D CAD drawing of the shaft-driven contra-rotating RPT with PTO, consisting of coaxial shafts and a bulb, housing the AF-PMSMs [27].

The RPT efficiency, excluding the hydraulic impact of the PTO, is higher for the shaft-driven RPT, experiencing a maximum of 90% in both pump and turbine mode [28]. As seen in section II the pump efficiency of the rim-driven RPT is only 84%. However, the main benefit of the shaftless rim-driven PTO concept is that any impact of the PTO on the hydraulic efficiency is evaded. Especially in a low-head PHS system with high flow rate, any secondary flow induction can induce significant losses. In the shaft-driven PTO design, two shafts are used to transfer mechanical torque and motion between the RPT runners and the AF-PMSMs. Each shaft is supported by two roller bearings, due to their high efficiency, high standardisation (for low diameter shafts) and low starting torque. In the rim-driven PTO design, the RPT runners are directly driven by AF-PMSMs designed around the runner rim, and the use of shafts is averted. However, due to the high diameter in the rim-driven PTO, active hydraulic bearings are proposed. Therefore, the bearing arrangement in the rim-driven PTO is more complex and has a higher cost than in the shaft-driven PTO. However, with proper maintenance, the reliability of this plain bearing arrangement can be significantly higher than its rolling elements counterpart. Next, the shaft-driven PTO only requires one high diameter mechanical face seal (3.5 m), lowering material and manufacturing cost and reducing leakage.

Next, the PTO mass and rotational inertia are compared. The PTO mass has a great influence on the radial loads in the bearing arrangement and gives an insight into material costs, while excessive rotational inertia can limit the dynamic capabilities of the RPT in a grid-supporting system. Table II lists the dimensional properties of the PTO of both the rim-driven and the shaft-driven CR RPT. Both AF-PMSMs of the shaft-driven PTO have a nominal power of 5 MW, with nominal rotational speeds of respectively 50 rpm and -45 rpm for the first and second runner. Note that the AF-PMSMs are water cooled in the shaft-driven PTO [27], which increases the stator current density and decreases its outer diameter D_o. The dimensional values for the rim-driven PTO are adopted from section III-B. One important parameter is the total magnet mass $2 \cdot m_m$, calculated by (5), as permanent magnets are experiencing a rapid increase in cost and are exhaustible. Although the AF-PMSM outer diameter D_o is significantly higher in the rim-driven PTO, the lower magnet height $D_o - D_i$ results in a similar total magnet mass for both concepts. Next, the total rotor disc mass $2 \cdot m_d$ and stator mass m_{st} are calculated. Contrary to the ring-shaped rotor discs and stator in the rim-driven AF-PMSMs with inner diameter equal to D_i, both the discs and stator in the shaft-driven AF-PMSM have an inner diameter equal to their shaft diameter D_s, increasing steel usage and weight. Furthermore, the shafts further increase the total PTO (rotor) mass and inertia. It can be concluded that the total PTO rotor mass m_r of the shaft-driven runners is more than three times higher than the total rotor mass of the rim-driven PTO, with the total PTO mass $m_{\mathrm{tot}} = m_r + m_{\mathrm{st}}$ being more than six times higher. However, due to the high diameter of the AF-PMSM in the rim-driven PTO, the rotational inertia is more than three times higher in this PTO. Therefore, it can be seen that for similar power ratings, the rim-driven PTO induces less radial loads and uses less core steel, but has a higher rotational inertia. Finally, the total PTO rotor mass and rotational inertia are compared to the RPT runners in a percentual increase, i.e., ${}^{m_r}/{}_{m_{\mathrm{runner}}}$ and ${}^{J_r}/{}_{J_{\mathrm{runner}}}$. From these values, it can be concluded that the percentual increases for both rotary mass and rotational inertia are significantly higher for the shaft-driven PTO.

V. Conclusions

In this paper, a PTO concept for a low-head 10 MW rim-driven contra-rotating RPT is proposed. The main benefit of this rim-driven RPT is that the full PTO is built around the periphery of the rim diameter. Therefore, the use of conventional shafts and any hydraulic impact of the PTO are averted. Two separate electric machines are used to directly drive the RPT runners. This allows a variable speed ratio and averts the use of a gearbox. Due to their high efficiency, power density and high diameter-to-length ratio, YASA topology Axial-Flux PMSMs are used. They are designed to suit the high diameter and low speed of the RPT. Although roller bearings are the common choice due to their high efficiency and low starting torque, reliability has proven to be an issue for roller bearings in multi-MW wind turbines. Furthermore, the high diameter of the discussed RPT increases initial cost. Active hydrostatic bearings are favorable for this PTO, as they combine the benefits of hydrostatic bearings under start-stop conditions and hydrodynamic bearings under nominal operation. A detailed analysis of the total cost of ownership for both high diameter roller bearings and active hydrostatic bearings is an interesting topic for future research. Finally, the derived rim-driven PTO is compared with the PTO of a shaft-driven contra-rotating RPT with similar power ratings and dimensions. Both the difference in hydraulic impact and bearing and sealing complexity is outlined. Notwithstanding the higher AF-PMSM diameter in the rim-driven PTO, both PTOs have a similar permanent magnet usage. Furthermore, it is shown that the rotary mass and the total mass of the rim-driven PTO is respectively three times and six times lower than that of the shaft-driven PTO. Future work includes the experimental validation of this rim-driven PTO using a model scale version.

Acknowledgment

This research is performed in context of the ALPHEUS project, which has received funding from the European Union's Horizon 2020 research and innovation programme under grant agreement No 883553. The authors would like to thank the European Union for funding this project.

References

[1] M. Qudaih, B Engel, D. P. K. Truijen, J. D. M. De Kooning, K. Stockman, J. Hoffstädt, A. Jarquin-Laguna, R. Ansorena Ruiz, N. Goseberg, J. Bricker, J. Fahlbeck, H. Nilsson, L. Bossi, M. Joseph, M. Zangeneh, "The contribution of low head pumped hydro storage to a successful energy transition," in *Virtual 19th Wind Integr. Workshop*, Darmstadt, Germany, Nov. 2020.

TABLE II
POWER TAKE-OFF MAIN PARAMETERS FOR BOTH THE RIM-DRIVEN AND THE SHAFT-DRIVEN CR RPT.

	Symbol	Rim-driven PTO		Shaft-driven PTO	
		Runner 1	Runner 2	Runner 1	Runner 2
AF-PMSM magnet outer diameter	D_o [m]	6.87		4.1	4.2
AF-PMSM magnet inner diameter	D_i [m]	6.4		3.28	3.36
AF-PMSM axial length	L_{AF} [m]	0.59		0.52	0.52
Total magnet mass	$2 \cdot m_m$ [kg]	350		338	354
Total disc mass	$2 \cdot m_d$ [kg]	$6.4 \cdot 10^3$		$11.3 \cdot 10^3$	$11.1 \cdot 10^3$
Total stator mass	m_{st} [kg]	$1.4 \cdot 10^4$		$1.1 \cdot 10^5$	$1.1 \cdot 10^5$
Shaft length / shaft diameter	L_s [m] / D_s [m]	/		6.4 / 0.65	2.7 / 0.77
Shaft mass	m_s [kg]	/		$1.2 \cdot 10^4$	$4.6 \cdot 10^3$
Total PTO rotor mass	m_r [kg]	$6.8 \cdot 10^3$		$2.4 \cdot 10^4$	$1.6 \cdot 10^4$
Total PTO mass	m_{tot} [kg]	$2.1 \cdot 10^4$		$1.4 \cdot 10^5$	$1.3 \cdot 10^5$
Total PTO rotational inertia	J_r [kg m²]	$7.46 \cdot 10^4$		$2.6 \cdot 10^4$	$2.6 \cdot 10^4$
Percentual rotary mass increase	$m_r / m_{\mathrm{runner}}$	11%	9%	40%	18%
Percentual rotational inertia increase	$J_r / J_{\mathrm{runner}}$	1.5%	1.2%	20.0%	12.5%

[2] J.-H. Kim, B.-M. Cho, S. Kim, J.-W. Kim, J.-W. Suh, Y.-S. Choi, T. Kanemoto, and J.-H. Kim, "Design technique to improve the energy efficiency of a counter-rotating type pump-turbine," *Renew. Energy*, vol. 101, pp. 647–659, Feb. 2017.

[3] T. Kanemoto and S. Obaz, "Proposition of unique pumping system with counter-rotating mechanism," *Int. J. Rotating Mach.*, vol. 10, no. 4, pp. 233–240, July 2004.

[4] S. Huang, J. Luo, F. Leonardi and T. A. Lipo, "A comparison of power density for axial flux machines based on general purpose sizing equations," *IEEE Trans. Energy Convers.*, vol. 14, no. 2, pp. 185–192, 1999.

[5] A. Cavagnino, M. Lazzari, F. Profumo, and A. Tenconi, "A comparison between the axial flux and the radial flux structures for PM synchronous motors," in *Proc. 2001 IEEE Ind. Appl. Conf. 36th IAS Annu. Meet.*, vol. 3, Chicago, IL, USA, Oct. 2001, pp. 1611–1618.

[6] G. Dubrovskiy, A. Mikerov, V. Dzhankhotov, and J. Pyrhonen, "General comparison of direct and geared drives for control applications," in *16th Eur. Conf. Power Electron. Appl.*, Finland, Aug. 2014, pp. 1–6.

[7] J. H. Kim and B. Sarlioglu, "Preliminary design of axial flux permanent magnet machine for marine current turbine," in *39th Annu. Conf. of the IEEE Ind. Electron. Soc.*, Vienna, Austria, Nov. 2013, pp. 3066–3071.

[8] P. Ojaghlu and A. Vahedi, "Specification and design of ring winding axial flux motor for rim-driven thruster of ship electric propulsion," *IEEE Trans. Vehicular Tech.*, vol. 68, no. 2, pp. 1318–1326, Feb. 2019.

[9] S. Djebarri, J. F. Charpentier, F. Scuiller, M. Benbouzid, and S. Guemard, "Rough design of a double-stator axial flux permanent magnet generator for a rim-driven marine current turbine," in *2012 IEEE Int. Symp. Ind. Electron.*, Hangzhou, China, May 2012, pp. 1450–1455.

[10] S. Djebarri, J. F. Charpentier, F. Scuiller, and M. Benbouzid, "Design and performance analysis of double stator axial flux PM generator for rim driven marine current turbines," *IEEE J. Ocean. Eng.*, vol. 41, no. 1, pp. 50–66, Mar. 2016.

[11] H. Vansompel, P. Sergeant, and L. Dupré, "Optimized design considering the mass influence of an axial flux permanent-magnet synchronous generator with concentrated pole windings," *IEEE Trans. Magn.*, vol. 46, no. 12, pp. 4101–4107, Aug. 2010.

[12] Advanced Design Technology Ltd, "TURBOdesign Suite version 2020R1," https://www.adtechnology.com/technology/turbodesign-suite/turbodesign-1(accessed May 23, 2022).

[13] M. Zangeneh, "A compressible three-dimensional design method for radial and mixed flow turbomachinery blades," *Int. J. Numer. Methods Fluids*, Sept. 1991.

[14] D. Kowal, P. Sergeant, L. Dupré, and A. Van den Bossche, "Comparison of nonoriented and grain-oriented material in an axial flux permanent-magnet machine," *IEEE Trans. Magn.*, vol. 46, pp. 279–285, Mar. 2010.

[15] J. Gieras, R.-J. Wang, and M. Kamper, "Sizing equations," in *Axial Flux Permanent Magnet Brushless Machines*, 1st ed. Berlin, Germany: Springer, 2005, pp. 54–57.

[16] A. El-Refaie and T. Jahns, "Scalability of surface PM machines with concentrated windings designed to achieve wide speed ranges of constant-power operation," in *IEEE Int. Conf. Elect. Machines and Drives*, San Antonio, TX, USA, Dec. 2005, pp. 1703–1709.

[17] J. Cros and P. Viarouge, "Synthesis of high performance pm motors with concentrated windings," *IEEE Trans. Energy Convers.*, vol. 17, no. 2, pp. 248–253, June 2002.

[18] P. B. Reddy, T. M. Jahns, and A. M. El-Refaie, "Impact of winding layer number and slot/pole combination on ac armature losses of synchronous surface pm machines designed for wide constant-power speed range operation," in *2008 IEEE Ind. Appl. Soc. Annu. Meet.*, Edmonton, AB, Canada, Oct. 2008, pp. 1–8.

[19] B. Wu and M. Narimani, *High-Power Converters and AC Drives, 2nd Edition*. Hoboken, NJ, USA: Wiley - IEEE Press, 2017, pp. 5–8.

[20] M. Preindl and S. Bolognani, "Optimized design of two and three level full-scale voltage source converters for multi-MW wind power plants at different voltage levels," in *37th Annu. Conf. IEEE Ind. Electron. Soc.*, Nov. 2011, pp. 3634–3639.

[21] V. H. J. Pyrhönen, T. Jokinen, *Design of Rotating Electrical Machines*, 1st ed. Hoboken, NJ, USA: Wiley, 2008.

[22] E. Hart, A. Turnbull, J. Feuchtwang, D. McMillan, E. Golysheva, and R. Elliott, "Wind turbine main-bearing loading and wind field characteristics," *Wind Energy*, vol. 22, no. 11, pp. 1534–1547, 2019.

[23] A. Rolink, T. Schröder, G. Jacobs, D. Bosse, J. Hölzl, and P. Bergmann, "Feasibility study for the use of hydrodynamic plain bearings with balancing support characteristics as main bearing in wind turbines," *J. Phys.: Conf. Ser.*, vol. 1618, pp. 1–10, Sept. 2020.

[24] W. Ur Rehman, Y. Luo, Y. Wang, G. Jiang, M. Iqbal, S. Urrehman, and S. Bibi, "Fuzzy logic–based intelligent control for hydrostatic journal bearing," *Measurement and Control*, vol. 52, Mar. 2019.

[25] A. Yadav and P. Pathak, "Control system for hybrid journal bearing: A fuzzy approach," *Recent Trends in Engineering Design, Lecture Notes in Mechanical Engineering,*, pp. 201–2010, June 2021.

[26] G. Ren and K. Ogle, "Hydro-turbine main shaft axial seals of elastic polymer – principle and practice," in *Waterpower XVI Conf.*, Spokane, WA, USA, 07 2009.

[27] D. P. K. Truijen, J. D. M. De Kooning, and K. Stockman, "Drivetrain architectures for a mechanically decoupled contra-rotating reversible pump-turbine," in *2021 IEEE/ASME Int. Conf. on Adv. Intell. Mechatron. (AIM)*, Delft, Netherlands, July 2021, pp. 7–12.

[28] J. Fahlbeck, H. Nilsson, S. Salehi, M. Zangeneh, and M. Joseph, "Numerical analysis of an initial design of a counter-rotating pump-turbine," *IOP Conf. Ser. Earth Environ. Sci.*, vol. 774, June 2021.